Induced Bias in Recovery of Spinning Neutron Star Binaries with Non-spinning Waveforms

Rachael Huxford

July 29, 2017

Induced Bias in Recovery of Spinning Neutron Star Binaries with Non-spinning Waveforms

Author: Rachael Huxford[1]
Mentors: A. Ghosh[2], C. Van Den Broeck[2]
[1] *Towson University, Towson, Maryland 21252, USA*
[2] *Nikhef, Science Park, 1098 XG Amsterdam, The Netherlands*
(Dated: July 24th, 2017)

Abstract

We continue the investigation of the feasibility of constraining the neutron star equation of state through gravitational waves. In particular, focus was on the ability to accurately recover tidal deformabilities of spinning waveforms using parameter estimation with non-spinning waveforms. We compare the match of TaylorF2 waveforms at the 3.5PN order with spin to the 2.0PN order and tidal effects to the 6PN order beyond leading order. It was shown that spin effects drastically decrease the match between two waveforms with increasing dimensionless spin values. We study the effects of a range of spin values in injected waveforms on the recovery of tidal deformabilty using non-spinning templates. Recovered tidal deformabilities were over and underestimated at high dimensionless spin values and effect sizes increased with increasing dimensionless spin values. Our analysis makes it known that recovering spinning waveforms with non-spinning ones renders recovery of tidal deformabilities highly inaccurate.

I. INTRODUCTION

Since the completion of Advanced LIGO, there have been three confirmed gravitational wave events detected from binary black hole mergers. With the impending completion of Advanced VIRGO and KAGRA as well as the possibility of LIGO-India, it is likely that detections will continue with increased sky position accuracy. Additionally, the approval of LISA may eventually provide sensitivities outside of current ranges and allow us to detect gravitational wave sources such as high mass binary black hole mergers, white dwarf binaries, and possibly even relics of the Big Bang. Moreover, as the sensitivities are improved in current ground-based detectors, it is possible that detections of not only binary black hole mergers (BBH) will occur, but also of binary neutron star mergers (BNS) and possibly neutron star-black hole mergers (NSBH) as well.

Gravitational waves of BBH coalescences have provided us with a wealth of scientific information. At the surface level, they have provided an indisputable proof of the existence of black holes. The first three detections have included both high and low mass systems which result in short and long waveforms respectively. These have been used to complete previously impossible tests of strong field general relativity such as those in references [1][2]. Gravitational waves from BNS mergers could prove to be no less valuable. These coalescences could be used to probe the neutron star equation of state (EOS) which, even today, remains mostly a mystery.

The EOS can appear in gravitational waveforms in many ways. The two primary sources of its appearance are the tidal deformations and the quadrupole-monopole effect, with the former being the focus of this paper. The tidal deformability of stars is related to the star's mass, m, in a way controlled by the EOS through the stars radius as: $\lambda(m) = \frac{2}{3}k_2(m)R^5(m)$, where k_2 is the second Love number. In the late stages of inspiral one star's tidal field $\mathcal{E}_{ij}$ generates a quadrupole moment Q_{ij} in the other. The generated quadrupole moment and tidal field source are related by the aforementioned tidal deformability $\lambda(m)$: $Q_{ij} = -\lambda(m)\mathcal{E}_{ij}$. The change in shape of the two neutron stars then has an effect on the orbit and thus, the emitted gravitational waveforms. This effect is most prominently seen in the phase $\Phi(f)$ and only at high orders of $(\frac{v}{c})$, but includes a fairly substantial factor [3]: $\lambda(m)/M^5 \propto (\frac{R}{M})^5 \sim 10^2 - 10^5$ where M is the total mass of the system as $M = m_1 + m_2$. This factor makes its impact noticeable at sufficiently high detector sensitivities, perhaps even at sensitivities already achieved in ground based detectors. Tidal deformation is not the only effect appearing in the phase, however.

The quadrupole-monopole effect is caused by a neutron star's spin. As the star spins, it becomes slightly oblate. Assuming a symmetric distribution about the axis of rotation, the deformed shape can be described by the quadrupole moment parameter: q. This parameter has been found to be linked to the dimensionless spin through a constant, a, where the constant is dependent on the mass as controlled

by the EOS [4]. The generated quadrupole moment then causes a coupling in its mass quadrupole moment with the mass of its binary, changing the gravitational potential. This change in gravitational potential appears in the emitted gravitational waveform through the phase in ways dependent on the post-Newtonian order as discussed later in this paper.

To model these effects, a great deal of time and effort has been put into numerical simulations of BNS mergers which can generate waveforms with fewer approximations in the late inspiral stage [5]. For the early inspiral stage, such complicated simulations are not needed, therefore simpler post-Newtonian approximations are used. The two models are then merged to form one coherent waveform. These waveforms are the most accurate representations of BNS systems made yet, but can take days to weeks to generate and millions of such waveforms are needed for effective data analysis of signals. This makes these waveforms impossible to use for current event detection and drives the study of possible alternatives.

This paper is a preliminary look into one such alternative solution using currently available waveform models. If the recovery templates used in parameter estimation do not account for the spin of the star, it is possible to reduce the generation time of advanced templates. Yet, one must consider the effect excluding spins will have on the effectiveness of the template. It is possible that recovering a waveform with spin using templates without it may introduce a bias in the results of the parameter estimation. However, this has yet to be proven and is therefore investigated here.

The following paper is formatted as such. In section (II) we discuss the model used to generate both template and injected waveforms as well as how the EOS of neutron stars affects that model. In section (III) we discuss the Bayesian analysis methods that are used in the parameter estimation of gravitational wave events as well as the match comparison of templates. Section (IV) covers the specific set-up and parameter space used in both the injection and recovery waveforms. Section (V) shows our main results. Section (VI) discusses these results and proposes possible further study.

In this paper c and G are equal to 1 unless stated otherwise.

II WAVEFORM APPROXIMANTS AND THE EFFECT OF NEUTRON STAR EOS

A. Waveforms Generated

We model gravitational waves using the stationary phase approximation (SPA) in order to get an expression for the gravitational wave strain. To do this, a Fourier transform of the waveform must be used in order to convert to the frequency domain. The SPA states that given a function $B(f) = A(t)\cos\phi(t)$, a good estimate of the Fourier transform is given by [6]:

$$\tilde{B} \simeq \frac{A(t_f)}{\sqrt{\dot{F}(t_f)}} e^{i[\Psi_f(t_f) - \frac{\pi}{4}]} \tag{1}$$

where $\Psi_f(t_f) \equiv 2\pi f t_f - \phi(t_f)$, f is the frequency, $F(t)$ is the instantaneous frequency of emitted radiation, and t_f is the time at which $F(t_f) = f$.

The Fourier frequency dependent waveform can then be shown to be:

$$\tilde{h}(f) = \mathcal{A} f^{-7/6} e^{i\psi(f)} \tag{2}$$

where $\mathcal{A} \propto \mathcal{M}^{5/6} Q(angles)/D$, D is the distance to the binary system in seconds, $\mathcal{M}$ is the chirp mass given by $\mathcal{M} = \eta^{3/5} M$, and *angles* include sky position as well as source orientation angles. The phase of the Fourier waveform is given by [6]:

$$\psi(f) = 2\pi f t_c - \phi_c - \frac{\pi}{4} + \frac{3}{128\eta\upsilon^5} \sum_{k=0}^{N} \alpha_k \upsilon^k \tag{3}$$

where $\upsilon = (\pi M f)^{1/3}$, η is the dimensionless mass ratio given as $\eta = m_1 m_2/M^2$, $k = 0, ..., N$ with $N = 7$ for the 3.5PN order and $N = 4$ for the 2.0PN order, and M is the total mass of the binary as stated previously. The coefficients for the phase are given by the values of α_i listed in Appendix A.

For the purpose of this paper, the phase was taken up to 3.5PN order with inclusion of spin to that order for parameter estimation and with inclusion of spin to the 2.0PN order for match comparisons. For spin affected α_i values, see Appendix A. For simplicity, we assumed that all spins were aligned or anti aligned with the direction of orbital angular momentum and with each other. The upper limit of all integrals was taken to be the GW frequency at last stable orbit before merger. For a point particle of mass M in Schwarzchild spacetime, this is given to be:

$$f_{lso} = \frac{1}{6^{3/2}\pi M} \tag{4}$$

Although the lower cutoff frequency is typically taken to be 20Hz, here it was taken as 40Hz. The effects of

tidal deformations do not appear until high frequencies, so the loss of the lower 20Hz was not considered theatrening to our results. More importantly, the reduction of frequency range significantly decreased the time of analysis. The lost 20Hz were not an especial subject of interest for this study therefore, to save time, they were not included.

Two effects of the EOS on waveforms were taken into account: the quadrupole-monopole effect, and tidal deformations. We will discuss these below.

B. Quadrupole-Monopole Effects

When a neutron star spins, it causes the star to deform and become slightly oblate. Assuming an axisymmetric mass distribution about the rotating axis, this change in shape forms a quadrupole moment which can become coupled with the mass monopole of its companion star. This coupling changes the gravitational potential and results in an alteration of the emitted gravitational radiation.

The quadrupole moment can be described by the dimensionless quadrupole moment parameter, q, given by [4]:

$$q = -\frac{5}{2}\lim_{r\to\infty}\left(\frac{r}{M}\right)^3\int_{-1}^{1}\nu(r,\theta)P_2(\cos\theta)d\cos\theta \quad (5)$$

where ν is a potential connected to the metric of the axisymmetric star, and P_2 is the second Legendre polynomial given by $P_2(x) = (3x^2 - 1)/2$. A stiffer EOS implies a larger radius, and, as can be seen in equation (5), the quadrupole moment parameter is dependent on the radius of the star. Therefore, q must also increase with increasing EOS stiffness. Estimates of q have been calculated numerically for varying EOS [7] and the results demonstrated the dependence of q on the dimensionless spin, χ. This relationship can be seen as:

$$q = -a\chi^2 \quad (6)$$

where a is a mass dependent parameter controlled by the EOS. Consequently, the EOS and the value of the dimensionless spin directly affect the quadrupole moment and hence the phase of emitted gravitational waves. For TaylorF2 wave approximations, this change in phase appears as factors in the Fourier coefficients of the phase. As can be seen in Appendix A, effects due to spin-orbit interaction first appear at 1.5PN order as a value of β [3] given by:

$$\beta = \frac{1}{12}\sum_{i=1}^{2}\left[113\left(\frac{m_i}{M}\right)^2 + 75\eta\right]\hat{L}\cdot\bar{\chi}_i \quad (7)$$

The spin-orbit effects then appear again along with spin-spin, and QM effects at 2.0PN as a factor of sigma [3] given by:

$$\sigma = \frac{\eta}{48}\left[-247(\bar{\chi}_1\cdot\bar{\chi}_2) + 721(\hat{L}\cdot\bar{\chi}_1)(\hat{L}\cdot\bar{\chi}_2)\right] \quad (8)$$

where $\hat{L}$ is the unit vector in direction of orbital angular momentum, $\bar{\chi}_i$ is the dimensionless spin vector for each star. QM effects to the 2.0 PN order and spin effects to the 2.5PN order in the time domain have also been calculated. These were included in our parameter estimation, but not our match comparison. See references [3], and [8] respectively for these values. As mentioned before, QM contributions are not the only source of alterations to the phase. Tidal deformations may also imprint important information on the phase of a gravitational wave.

C. Tidal Deformations

During the late stages of inspiral, the tidal tensors, $\mathcal{E}_{ij}$, of one star can induce a quadrupole moment Q_{ij} in the other. With an adiabatic approximation, the two are related by:

$$Q_{ij} = -\lambda(m)\mathcal{E}_{ij} \quad (9)$$

where m is the mass of the star with the induced quadrupole, and λ is the tidal deformability determined by the EOS and dependent m. The induced quadrupole moment can change the shape of the affected star, altering the orbital motion. The phase of the emitted gravitational waves is thus altered as well, carrying away information about its progenitor star. The change in phase caused by these tidal effects can be seen as [9]:

$$\Psi(\upsilon) = \Psi_{PP}(\upsilon) + \Psi_{tidal}(\upsilon) \quad (10)$$

where υ is the characteristic velocity given by $\upsilon = (\pi M f)^{1/3}$, Ψ_{PP} is the phase from the inspiral of a point particle, Ψ_{tidal} is the tidal effect's contribution to the phase. The tidal effects contribution alone appears as [9]:

$$\Psi_{tidal}(\upsilon) = \frac{3}{128\eta}\upsilon^{-5}\sum_{i=1}^{2}\frac{\lambda_i}{M^5\chi_i}\Bigg[-24(12-11\chi_i)\upsilon^{10} + \frac{5}{28}(3179-919\chi_i-2286\chi_i^2+260\chi_i^3)\upsilon^{12} \tag{11}$$
$$+ 24\pi(12-11\chi_i)\upsilon^{13}$$
$$- 24\left(\frac{39927845}{508032} - \frac{480043345}{9144576}\chi_i + \frac{9860575}{127008}\chi_i^2 - \frac{421821905}{2286144}\chi_i^3 + \frac{4359700}{35721}\chi_i^4 - \frac{10578445}{285768}\chi^5\right)\upsilon^{14}$$
$$+\frac{\pi}{28}(27719-22127\chi_i+7022\chi_i^2-10232\chi_i^3)\upsilon^{15}\Bigg]$$

Where $\chi_i = m/M$, $i = 1, 2$, $\lambda = \lambda(m_i)$, M is the total mass, and $\eta = m_1 m_2/M^2$. These tidal effects only appear starting at the large post-Newtonian order of 5PN [9]. Nonetheless, their large factors are on the scale of two to five orders of magnitude which may allow us to possilby gain information about the EOS of their sources.

III DATA ANALYSIS

A. Match Comparison

All templates and waveforms were generated using the TaylorF2 approximation to the 3.5PN order including spin to the 2.0PN order when applicable. To compare waveforms, the match was defined in the frequency domain as:

$$Match = \frac{(h_i|h_j)}{\sqrt{(h_i|h_i)}\sqrt{h_j|h_j}} \tag{12}$$

where $\tilde{h_i}$ is defined as the strain of the waveform, and i, j are the spin values. This value serves as a quantitative value of correlation between two vectors or in our case, waveforms. A match of one signifies identical waveforms, while for a match of zero, or less, the opposite is true. The inner product is defined as below:

$$(h_i|h_j) = 4Re\int_{flow}^{flso}\frac{\tilde{h_i}^*(f)\tilde{h_j}(f)df}{S_h(f)} \tag{13}$$

where $\tilde{h_i}^*(f)$ is the complex conjugate of $\tilde{h_i}(f)$, and $S_h(f)$ is the power spectral density distribution.

B. Parameter Estimation

The foundation for the process of parameter estimation is Bayes' theorem. Given two events, A and B, the probability of them both occurring is the probability of B occurring given that A has occurred multiplied by the probability of A occurring alone. This can be represented by the statement:

$$P(A \wedge B) = P(B|A)P(A) \tag{14}$$

Bayes' theorem then says that the probability of both occurring given that A has already occurred is equal to the probability of both occurring given that B has already occurred. This can be shown as:

$$P(A \wedge B) = P(B \wedge A)$$
$$P(B|A)P(A) = P(A|B)P(B)$$
$$P(B|A) = \frac{P(A|B)P(B)}{P(A)} \tag{15}$$

However, it is often necessary to begin with a set of assumptions, I. For example, these assumptions can include maintaining that the mathematics one uses is accurate, or claiming a curved spacetime. Presuming they are correct, equation (13) then becomes:

$$P(B|A, I) = \frac{P(A|B, I)P(B|I)}{P(A|I)} \tag{16}$$

In our analysis, this process was used given that events A and B are parameters, θ, and data, d. Here, the data consists of the waveform and noise, and θ represents masses, spins, sky position, orientation, distance, time of coalescence, and phase at coalescence. Replacing A and B with θ and d respectively gives:

$$P(\theta|d, I) = \frac{P(d|\theta, I)P(\theta|I)}{P(d|I)} \tag{17}$$

where $P(\theta|d, I)$ represents the posterior density function, $P(d|\theta, I)$ the likelihood function, $P(\theta|I)$ the prior probability density, and $P(d|I)$ the evidence. The prior probability density represents the probability of the parameters θ corresponding to that of an observation, before having considered the data from an observation. This prior probability may take into account previous knowledge such as known astrophysical mass ranges, or estimated tidal deformability ranges. The likelihood can be described as the probability of the data, d, containing the parameters, θ, while also being observed as an event and has been previously shown [3] to be:

$$P(d|\theta, I) = \mathcal{N}e^{\left[-2\int_{f_{lso}}^{f_{low}} df \frac{|\tilde{d}(f)-\tilde{h}(f,\theta)|^2}{S_n(f)}\right]} \tag{18}$$

where $\mathcal{N}$ is a normalization constant, $\tilde{d}$ is the Fourier transform of the data, $\tilde{h}$ is the frequency domain

waveform, and $S_n(f)$ is the power spectral density.

This likelihood function was calculated and implemented through a nested sampling technique. In this technique, a parameter space is constructed with as many as seventeen dimensions for BNS systems. Random 'seed' points are then distributed throughout this space and the likelihood as well as the posterior probability is calculated at each. Then, each point is moved in a random direction within a determined range and both functions are calculated again. This process continues until a maximum is converged upon and all calculated points are returned to form a posterior density distribution. The maximum of this distribution is then the recovered parameter set.

IV. SIMULATIONS

A. Match Comparison

All templates and waveforms were generated using the TaylorF2 approximation to the 3.5PN order including spin to the 2.0PN order when applicable. Four waveforms were generated and compared: with no spin, with only spin, with only tidal effects, and with spin and tidal effects. The two masses were taken to be equal to a known average of $1.4M_\odot$ and were given to be the same across waveform type. The dimensionless $\Lambda_i = \lambda(m_i)/m_i^5$ value was taken to be a constant of 1690, well within the reasonable range for neutron stars of dimensionless $\Lambda \in [50, 5000]$.

The $Q(angles)$ gets eliminated from the match formula, and was therefore set to a placeholder of one. We were not interested in the effects the extrinsic parameters may cause, so the time of coalescence and the phase at coalescence were taken to be a constant 0.01 seconds and 0.01 radians respectively. Additionally, the lower cutoff frequency was given as $f_{low} = 20Hz$ in order to include as much of the waveform as possible while considering the sensitivity of the detectors.

B. Injections

All injection files were made in the eos_dev branch of the simulation code. However, this branch did not include the ability to introduce spin values in injections without changing other parameters, nor did it allow us to generate and inject tidal deformabilities dependent on the EOS. Therefore, after an injection file was generated, a script was executed. This script edited the injection file, allowing desired spin and tidal deformability values. Additionally, changes had to be made to the parameter estimation code to allow reading of the injected tidal parameters in the frequency domain. Initially, this was only available in the time domain.

As a reference for the parameters chosen in the injection waveforms, we used known neutron star data. For obvious reasons, the sky location (θ, φ) and orientation (ι, ψ) are both distributed uniformly on the sphere. Knowing that the average known neutron star in a binary falls in the range $m \in [1, 2]M_\odot$, the mass distribution for both stars was given as uniform in a mass range $m_i \in [1.1, 1.6]M_\odot$. Choosing it as such provides our chosen range with a wide scope of possible stars without uneccesarily increasing computing time.

The fastest known pulsar in a binary system rotates with a dimensionless spin value of ~ 0.02. Therefore, a range of $\chi_i \in [-0.05, 0.05]$ more than accounts for all known spins of neutron stars in binaries. To test the limits, we also included a range of $\chi_i \in [-0.5, 0.5]$, and $\chi_i = 0$ as a control to compare to. Including ranges of both positive and negative values allows for the spins to be aligned, or anti-aligned with each other and the direction of orbital angular momentum in the z-direction only. Other alignments were not considered in this paper, but they make logical platforms for any future study.

To probe our ability to distinguish between stiff and soft EOS in recovery, a range of EOS was injected. The EOSs chosen were MS1, H4, and SQM3 which correspond to stiff, moderate, and soft respectively. These EOS were then used to calculate the injected Λ values based on the mass.

The generated waveforms were injected into simulated standard noise from Advanced Virgo in Italy, and the Advanced LIGO detectors in Lousiana and Washington states. As the effect of noise on recovery was not the focus of this study, we set a range of $SNR \in [15, 50]$. This is a typical SNR range known to allow detection of binary systems.

C. Recovery

Prior distributions of parameters were chosen to be the following. A TaylorF2 waveform to the 3.5PN order was assumed. The IFOs of Advanced Virgo, LIGO Lousiana and LIGO Washington were used for analysis with a lower frequency cutoff of 40Hz. All spins were set to $\chi_i = 0$ to investigate the bias of recovering spinning waveforms using templates without spins.

Mass was allowed as a flat component distribution $m_i \in [1.0, 1.7]M_\odot$. A flat distribution was chosen over a Gaussian because the mass distribution of neutron stars is not confidently known. Too few observations of these systems have been done in order to

assume anything but an even distribution [3]. In the recovery of tidal deformability, EOS were not chosen. Instead, tidal deformability was presumed in a distribution of $\Lambda \in [50, 5000]$ for injected SQM3 and H4 EOS. However, it was discovered that this range was limiting for the stiffest injected EOS: MS1. Therefore, for runs done with the injected MS1 EOS, the prior range was set to $\Lambda \in [50, 10000]$.

From the posterior samples, a comparison was made between the recovered dimensionless Λ value and the injected. This comparison can be seen as:

$$\Sigma = \frac{\Lambda_{rec} - \Lambda_{inj}}{\sigma_{rec}} \tag{19}$$

where Σ is called the effect size, σ_{rec} is the standard deviation of the recovered dimensionless Λ, and Λ_{rec} and Λ_{inj} are the recovered and injected dimensionless Λ values accordingly. This relation shows any systematic offsets in the measurement of Λ quantitatively. These values are listed as 'effect size' in the figures below.

V. RESULTS

A. Effects of spin on matched filtering

Four waveforms were compared: non-spinning, non-spinning with tidal effects, spinning, and spinning with tidal effects. Each of these waveforms were taken to the 3.5PN order including spin to the 2.0PN order in the frequency domain. Examples of these waveforms can be seen below in Figure 1.

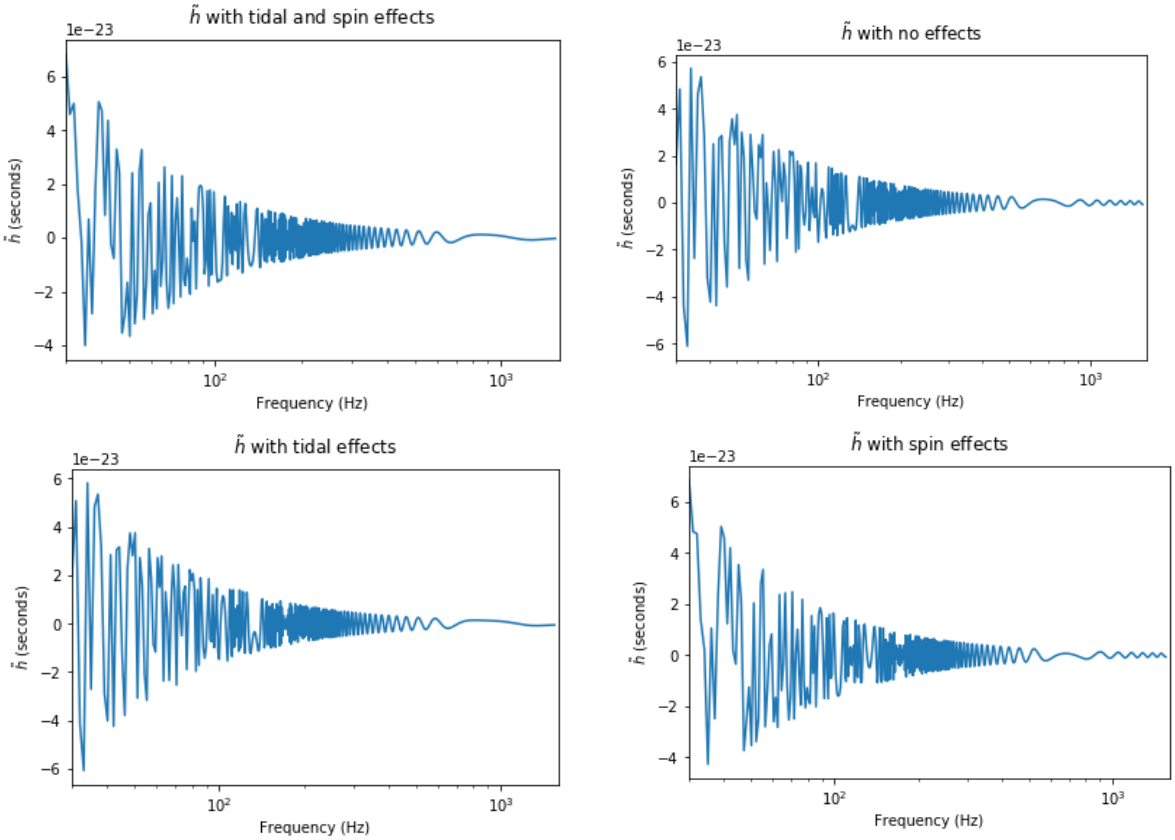

Figure 1: TaylorF2 waveforms used in a match comparison analysis.

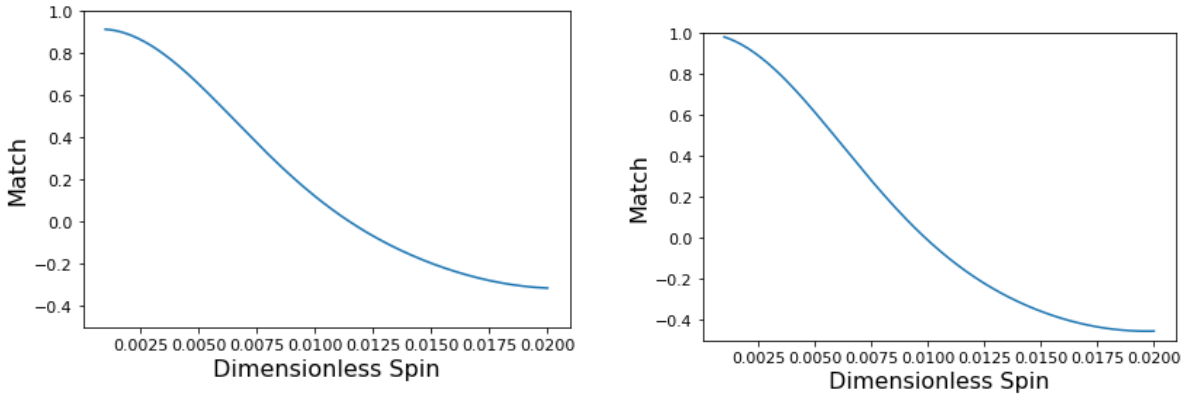

(a) (b)

Figure 2: Matched filtering results of a range of spin values [0,0.02]. (a) The matched result of a template with spinning and tidal effects with $\Lambda = 1690$. (b) The matched result of a template including spin, but not tidal effects.

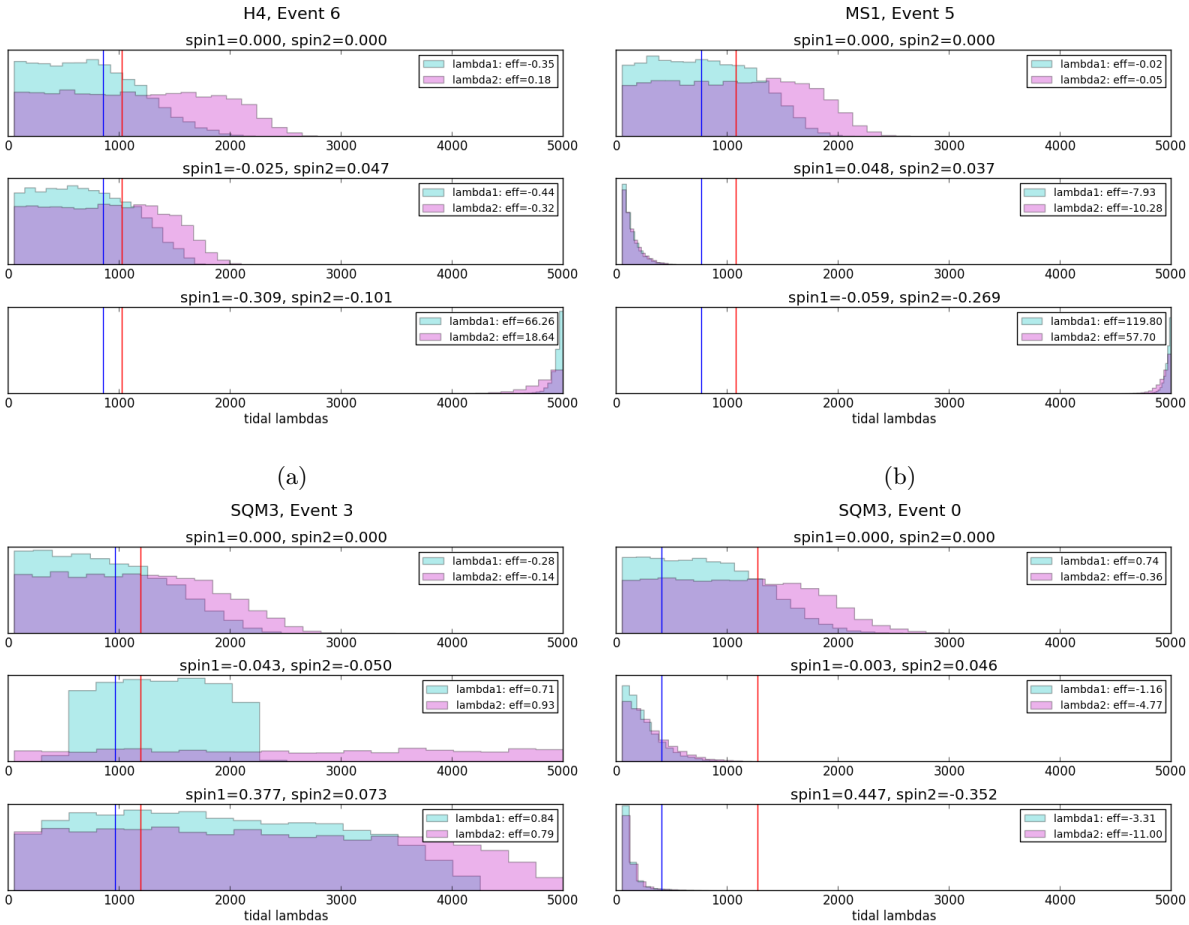

(a) (b)

(c) (d)

Figure 3: Examples of posterior parameter estimation of the dimensionless Λ value.(a)In bottom panel, an overestimation of recovered parameters appears with high spin. (b)In the middle panel, an underestimation of parameters appears with medium range spin. (c) A flat distribution across Λ appears in the middle and bottom panels with large spin. (d) Underestimation seen in middle panel for both Λ even though one injected spin is small.

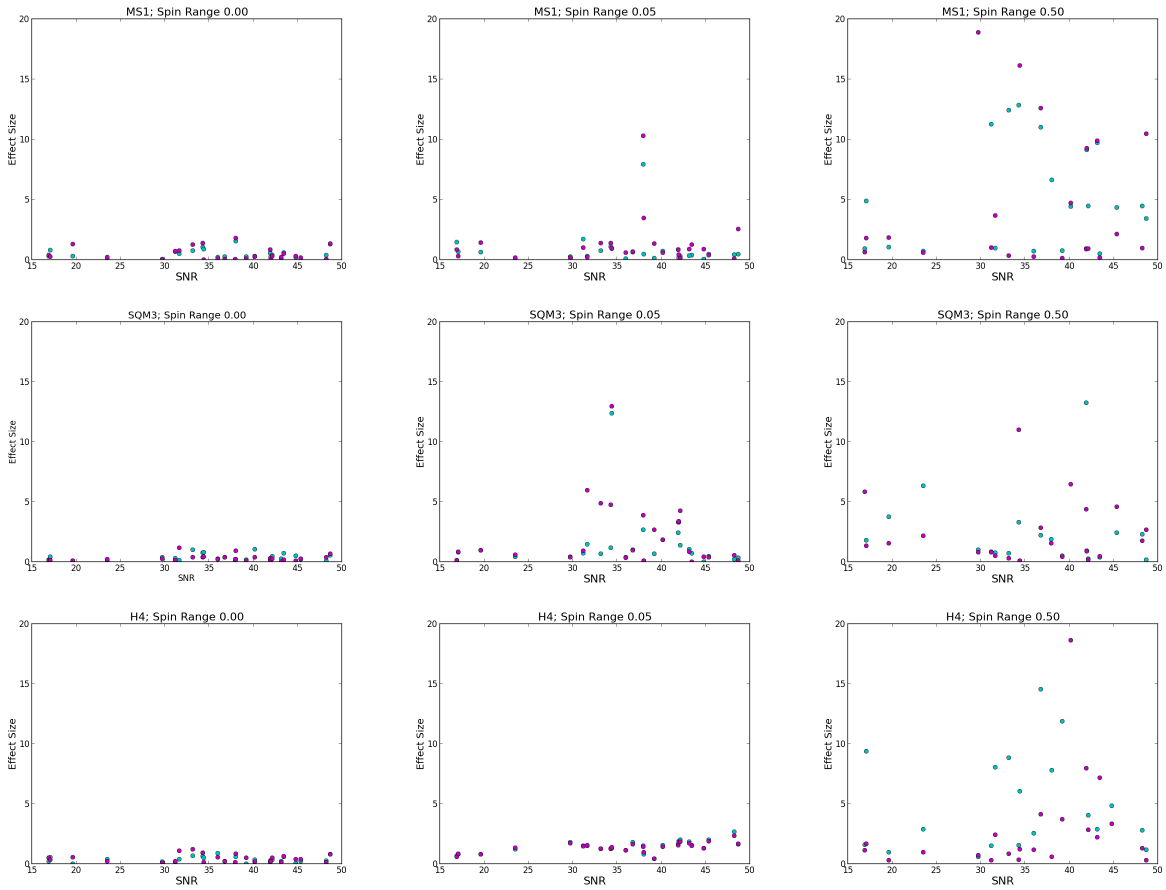

Figure 4: All injected spin values of each star in all three spin ranges, for each EOS. (a) EOS: MS1 (b) EOS: SQM3 (c) EOS: H4

It can be seen by the naked eye that the waveforms are different, but the match provided quanitative proof of this. Each of the waveforms that included spin effects were matched with the unaffected waveform with increasing values of spin. As can be seen in Figure 2, the match value drops to one half at spins as low as $\chi = 0.0058$ and to zero for spins as low as $\chi = 0.0098$ for this model. It was also found that including tidal effects as well as spin produces an even greater decrease in the match, and therefore an even larger departure from the original waveform. This can be seen in the lowering of the upper bound between (a) and (b).

B. Bias in recovery of spinning waveforms using non-spinning templates

Batches of twenty-five injections for each of three spin sets, and three EOS were run with a recovery that used templates without spin. Examples of the posterior samples can be seen in Figure 3 for a range of EOS and spin. Many high spin value runs returned results similar to that of (a) with injected spins of -0.309 and -0.101. Here, the high injected spin value caused an extreme overestimation of the injected Λ values. Similarly, high injected spins were also found to cause an extreme underestimation of injected Λ values, such as that in (b) with injected spins of 0.048 and 0.037. Additionally, if only one star had a high injected spin, both stars' parameters were recovered incorrectly with large effect sizes. This can be seen in the middle panel of (d) and (d).

A relation can be drawn between the effect size and the injected spin values as seen in Figures 4 and 5. In Figures 4 and 5, it can be seen that with no spin, the effect size remain very close to zero. However, as the spin increases, so does the effect size. As seen in Figure 4, it was found that even in the range of spin from [-0.05,0.05] some large effect sizes already occur. As the range increases to [-0.5,0.5], the effect size only increases. It also becomes obvious in Figure 4 that this is true regardless of EOS.

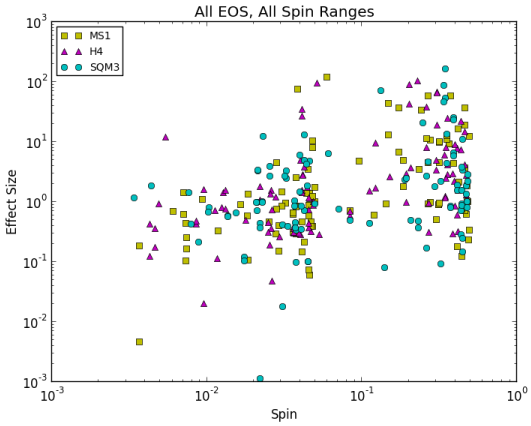

Figure 5: All injected spin values of each star in all three spin ranges, for each EOS. (a) EOS: MS1 (b) EOS: SQM3 (c) EOS: H4

Figure 5 only futhers these results. This figure makes it obvious that increasing spin does indeed result in increasing effect size. Yet, it cannot be determined from these results if the relation between spin and effect size is linear, or otherwise. Additionally, at a spin of 0.0377 it was found that 90% of values have an effect size of less than two. This means that 0.0377 is the maximum spin at which most of the recovered parameters are less than two standard deviations away from the injected values.

VI: DISCUSSION

We have continued the study into the possibility of determining the EOS of a neutron star by its gravitational wave signal. Our main focus was an initial inquiry into the feasability of accurately recovering tidal parameters from spinning neutron stars using non-spinning waveforms. The foundation we used for our analysis were the match comparison and the Bayesian analysis method of parameter estimation. Match comparison allowed us to analyze the effect spin and tidal effects had on the amplitude of strain. It was found that spin highly affected the generated waveforms. Spin values as low as $\chi_i = 0.0058$ decreased the match between a spinning and non-spinning waveform to 0.5. This stood as a proof of concept for the rest of the study, and encouraged further investigation.

Parameter estimation with different prior and injected spin values was completed for a stiff (MS1), moderate (H4), and soft (SQM3) EOS. It was found that spin severely affected the accuracy of recovery of tidal deformability values. High spins often caused either a gross over or underestimation, and occasionally returned a flat distribution. It was seen that at spins above 0.0377, recovered parameters began to recover values more than two standard deviations from the injected ones. Thus, spins outside of the 0.05 range were rarely seen to return any information of value. Luckily, this is outside of the known astrophysical range of spins for pulsars in binary systems. However, this is still essential to future efforts of modeling binary neutron star systems and one should be aware of the recovery biases when modeling spinning systems.

As mentioned before, this was only an initial inquiry into these effects, and stands as a proof of concept for further study with more advanced waveform models not currently available. With only these simple models at hand, precession and non-aligned spins would prove to be a solid foundation for prospective work.

Acknowledgements:
R.H. is supported by the National Science Foundation: Research Experience for Undergraduates. R.H. would like to thank the University of Florida for organizing the research experience, and assisting with international travel. She would also like to thank her mentors and colleagues at Nikhef for providing a welcoming, and supportive work environment. In particular, she would like to thank Archisman Ghosh for his constant support and mini lessons on a variety of data analysis topics. Additionally, she would like to thank Gregorio Carullo for the multiple instructional coding documents and sessions without which she would still be struggling to use the command line.

Appendix A

Fourier Phase Coefficients [6]:

$$\alpha_0 = 1,$$
$$\alpha_1 = 0,$$
$$\alpha_2 = \frac{20}{9}\left(\frac{743}{336} + \frac{11}{4}\eta\right),$$
$$\alpha_3 = -16\pi,$$
$$\alpha_4 = 10\left(\frac{3058673}{1016064} + \frac{5429}{1008}\eta + \frac{617}{144}\eta^2\right),$$
$$\alpha_5 = \pi\left(\frac{38645}{756} + \frac{38645}{252}\log\left(\frac{\upsilon}{\upsilon_{lso}}\right) - \frac{65}{9}\eta\left[1 + 3\log(\frac{\upsilon}{\upsilon_{lso}}\right]\right),$$
$$\alpha_6 = \left(\frac{11583231236531}{4694215680} - \frac{640\pi^2}{3} - \frac{6848\gamma}{21}\right) + \eta\left(-\frac{15335597827}{3048192} + \frac{2255\pi^2}{12} - \frac{1760\theta}{3} + \frac{12310\lambda}{9}\right)$$
$$+ \frac{76055}{1728}\eta^2 - \frac{127825}{1296}\eta^3 - \frac{6848}{21}\log(4\upsilon),$$
$$\alpha_7 = \pi\left(\frac{77096675}{254016} + \frac{378505}{1512}\eta - \frac{74045}{756}\eta^2\right)$$

where $\eta = \frac{m_1 m_2}{M^2}$, υ is the characteristc freqency, υ_{lso} is the frequency of last stable orbit, *gamma* is Euler's constant = 0.577, $\theta = -1.28$, and $\lambda = -0.6451$

Spin Effected Fourier Phase Coefficients [3]:

$$\alpha_0 = 1,$$
$$\alpha_1 = 0,$$
$$\alpha_2 = \frac{20}{9}\left(\frac{743}{336} + \frac{11}{4}\eta\right),$$
$$\alpha_3 = (-4\pi - \beta),$$
$$\alpha_4 = 10\left(\frac{3058673}{1016064} + \frac{5429}{1008}\eta + \frac{617}{144}\eta^2 - \sigma\right)$$

References

[1] T. L. S. Collaboration and the Virgo Collaboration, "Tests of general relativity with gw150914,"

[2] M. Agathos, W. D. Pozzo, T. G. F. Li, C. V. D. Broeck, J. Veitch, and S. Vitale, "Tiger: A data analysis pipeline for testing the strong-field dynamics of general relativity with gravitational wave signals from coalescing compact binaries,"

[3] C. V. D. Broeck and A. S. Sengupta, "Binary black hole spectroscopy,"

[4] M. Agathos, J. Meidam, W. D. Pozzo, T. G. F. Li, M. Tompitak, J. Veitch, S. Vitale, and C. V. D. Broeck, "Constraining the neutron star equation of state with gravitational wave signals from coalescing binary neutron stars,"

[5] D. Radice, L. Rezzolla, and F. Galeazzi, "High-order numerical-relativity simulations of binary neutron stars,"

[6] K. G. Arun, B. R. Iyer, B. S. Sathyaprakash, and P. A. Sundararajan, "Parameter estimation of inspiralling compact binaries using 3.5 post-newtonian gravitational wave phasing: The non-spinning case,"

[7] W. G. Laarakkers and E. Poisson, "Quadrupole moments of rotating neutron stars,"

[8] K. G. Arun, A. Buonanno, G. Faye, and E. Ochsner, "Higher-order spin effects in the amplitude and phase of gravitational waveforms emitted by inspiraling compact binaries: Ready-to-use gravitational waveforms,"

[9] W. D. Pozzo, T. G. F. Li, M. Agathos, C. V. D. Broeck, and S. Vitale, "Demonstrating the feasibility of probing the neutron star equation of state with second-generation gravitational wave detectors,"